Henryk Kapusta

Technical University of Łódź
Faculty of Textile Engineering and Marketing
Department of Technical Mechanics
ul. Żwirki 36, 90-924 Łódź, Poland
E-mail: biuro_nauki@cenaro.lodz.pl

Analysis of the Dynamics of a Double-Crank Driving Unit for a Needle Bench

Abstract
This article comprises the physical modelling and mathematical description of the double-crank driving unit of a needle bench, and the identification of the working conditions which directly influence the kinetics of this mechanism. A physical model in the form of a structural system was developed for the considerations related to the dynamics of the driving unit. The mathematical model elaborated describes the whole electromagnetic system including the dynamics of the asynchronous motor and the mutual interactions of the mechanical and the electrical parts.

Key words: *needle-punching machine, needle bench, driving unit, double crank, modelling, dynamics, simulation.*

Introduction

The broad application of nonwoven products has influenced the development of manufacturing techniques for this textile branch. The nonwoven textile manufacturing branch has generated not only new production methods, but also new, hitherto unknown, machines for production and has also influenced the development of new modifications of traditional machines. Needle-punching machines belong to these latter constructions. They have grown to be more and more complex with high-quality working parameters, but also with great sensitivity to faults during exploitation.

The recognition of the dynamic properties of needle-punching machines is a difficult task. The complex driving unit is the cause of this difficulty. This unit includes an asynchronous motor, a belt transmission, toothed gears, and a crank-slider mechanism connected to the needle-bench.

Thus, in the case of needle-punching machines, it seems most advantageous to carry out simulation tests with the use of a mathematical model of the needle-punching machine which is able to describe the whole electromagnetic system. This system must take into consideration the dynamics of the asynchronous motor and the mutual interactions of the mechanical and electrical parts, and must also determine the effects of changes - consciously introduced into the system - to the construction parameters of both the above-mentioned parts.

The Physical Model

A physical model of a real driving system is based on the structural scheme of the needle-bench driving unit. The idealised physical model accepted by us and presented in Figure 1 is a discrete model.

Only a comparison of the results of analytical analysis with the experimental data can prove whether the real system units accepted during modelling can be idealised. In the physical model accepted, system elements such as toothed wheels, shafts, vee-belts, etc., are modelled as elasto-dissipative elements. Some properties of the kinematic chain links, such as the coefficient of elasticity k and the dumping coefficient c, are marked at the related elements in Figure 1.

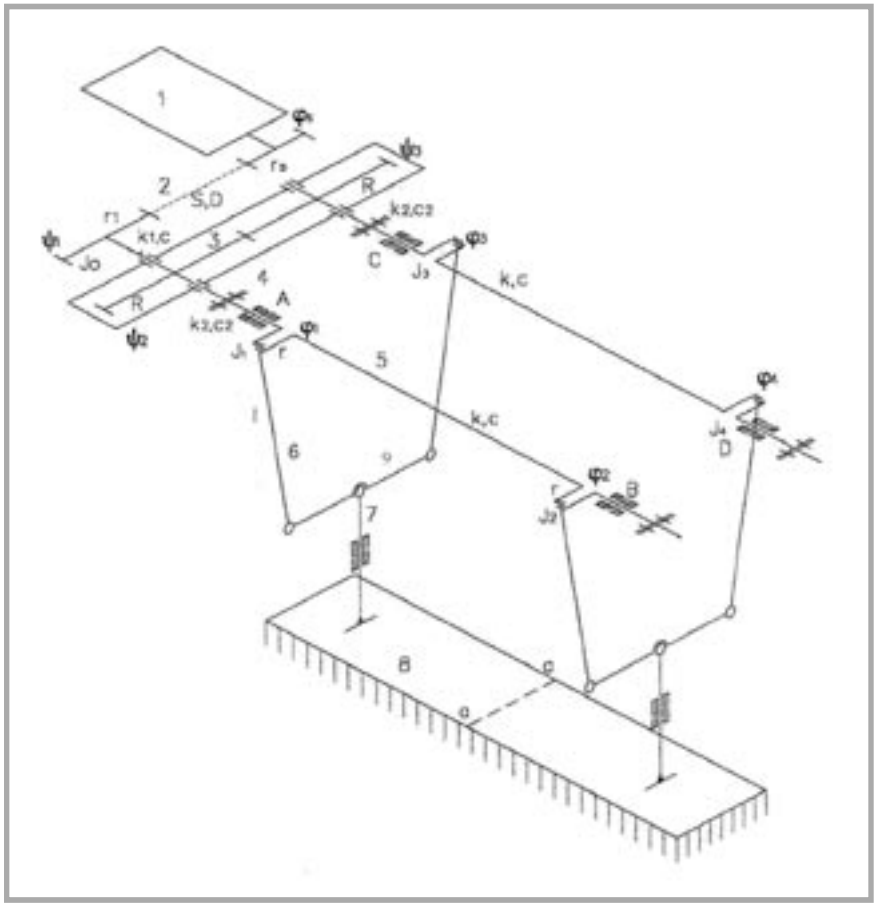

Figure 1. *Structural scheme of the needle-bench driving unit: 1 - motor, 2 - belt transmission, 3 - toothed gear, 4 - clutch, 5 - main shaft, 6 - crank-slider mechanism, 7 - slider, 8 - needling bench, 9 - lever; A, B, C, D - nodes, J_0 - mass moment of inertia of the belt wheel, J_1 ... J_4 - mass moments of inertia, c - shaft dumping coefficient, c_2 - dumping coefficient, K_1 - shaft rigidity of the toothed gear, K_2 - shaft rigidity, S - belt rigidity, D - belt dumping coefficient, r - crank radius, r_S - radius of the motor belt-wheel, r_1 - radius of the belt wheel (belt transmission), R - radius of the toothed wheel, l - length of the connector rod, ψ_1 ... ψ_3 - rotation angles of the wheels, φ_1 ... φ_4 - mass rotation angles.*

Modelling the dissipative properties of the particular elements is one of the most complex tasks. This is caused by the lack of accurate mathematical descriptions of dissipative phenomena. The non-linear character of the dissipative forces, for example those of mixed friction, which can appear in the sliders guiding the needle bench, significantly influences the dynamic system properties.

The majority of the needle-punching machines used today have a crank-slider driving unit. Such mechanisms have been analysed in detail in work [1], as well as in further works which are related mainly to the crank mechanisms of combustion engines. The publications [2-5] include analyses of the dynamics of mechanisms in which the torsion oscillations are induced as the result of the reciprocating movements of the working elements. The author's own works [6-10] consider the dynamics of the needle-punching machine's driving unit, and include analyses of the occurring phenomena with consideration of the technological resistance.

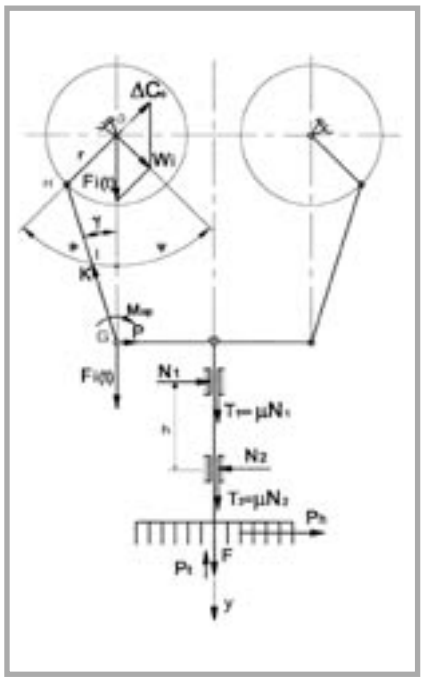

Figure 2. *Distribution of forces acting in the crank-slider mechanism: $F_i(t)$ - inertial force of masses connected with the needle bench, K - interaction force of connector rod acting on the cross-bar, ΔC_o - centrifugal inertia force, N_1 and N_2 - normal forces, T_1 and T_2 - friction forces, P_t - force of technological resistance, P_h - nonwoven tension force, W_i - resultant force, M_{op} - bolt moment of friction, r - crank radius, l - length of connector rod, T_i - resistance force of slider friction, μ - coefficient of friction, φ - crank rotation angle, ψ - angle of the resultant force position h - distance between the brushes.*

The driving unit system shown in Figure 1, which has been accepted for the analysis presented, was developed as the result of systems discussed earlier. The d'Alembert principle of virtual works was used to describe the system's kinetics. This method offers a number of advantages, especially for designers and operating staff.Principally, it enables the determination of forces which are the basis for strength calculations of system elements, including calculation of bearings.

Force Distribution in the Crank-slider System

The force distribution in the crank-slider system is presented in Figure 2. Taking into account the system's symmetry, it is sufficient to consider only the forces acting on one of both the crank-sliders' mechanisms. From the OHG triangle (Figure 2) we have:

$$l\sin\gamma_i = r\cdot\sin\varphi_i$$

hence:

$$\cos\gamma_i = \sqrt{1-\lambda^2\sin^2\varphi_i}$$

and

$$\gamma_i = arc\cos\sqrt{1-\lambda^2\sin^2\varphi_i} \qquad (1)$$

From the equilibrium of the G node we have:

$$K_i = \frac{F_i(t)-\mathrm{sgn}(\dot{y}_i)T-P_t}{\sqrt{1-\lambda^2\sin^2\varphi}} \qquad (2)$$

where:

$$\lambda = \frac{r}{l} \qquad (3)$$

The axial forces which are acting in the G node equal:

$$F_i(t) = -m\frac{d^2y_i}{dt^2} - \mathrm{sgn}(\dot{y}_i)T_i - P_t \qquad (4)$$

The force $P_t \neq 0$, only for the range of

$$310° \le \tau \le 360°.$$

The friction force T_i of the slider can only be estimated. Theoretically, considering the system's symmetry, the force should equal zero; but in reality it is dependent on the accuracy of manufacturing the crank, the cross-bar, and the connector rod, as well as on the influence of the bench's inertia forces, and the forces of the collected nonwoven's interaction on the slider. A constant value of T_i can be accepted for calculation. The sense of friction force T_i is opposite to the velocity $\dot{y}_i$ and compatible with -sgn($\dot{y}_i$). This sense changes twice during one crank revolution.

As the result of continuously receiving the nonwoven, the formation of nonwoven tension is generated during the whole time that the needles are in contact with the nonwoven. The nonwoven is stopped in the needling area, whereas the take-up rollers cause the continuous movement of the jammed end. The horizontal force P_h generated by the tension, which increases as the needles sink (a continuous increase in tension occurs), is transmitted by the needles and by the friction of the nonwoven to the perforated plate. A part of the fleece fibres is pressed into the openings of the perforated plate, which increases the participation of the bottom perforated plate in the transmission of horizontal technological forces. The moment of friction on the bolt fastening the connector with the cross-bar is formulated by:

$$M_{iop} = K_i\mu\frac{d_1}{2} \qquad (5)$$

where:

M_{iop} - the moment of friction on the bolt fastening the connector with the cross-bar (point G),
μ - the coefficient of friction, and
d_1 - the bolt diameter.

Values of the Moments of Friction M_i

All the elements of the driving shaft, i.e. all the elements mounted to the shaft, whose rotational axes are compatible with the shaft axis, are dynamically balanced in their reciprocating motion. The elements with mass centres concentrated at the crank journal axis (at the eccentric) generate the formation of centrifugal inertia forces

$$\Delta C = m_0 r\omega^2$$

and are balanced by the main counterweights.

The inertia resistances of the masses in linear motion acting along the way of the slider can be designated as axial inertia resistances, in contrast to the centrifugal forces. Independently of the inertia resistances, other axial forces exist, such as the force of slider friction and the technological impulse forces acting over time as the needles pierce the fleece.

It is impossible to obtain the total mass balance in linear reciprocating motion in the needle-bench driving unit using the main counterweights, as the resistances in linear motion have a constant direction but a variable absolute value, whereas the centrifugal forces have a constant

absolute value but a variable direction. However, the possibility exists of a partial force balance in linear motion by the main counterweights.

A decrease (moderation) in the mass inertia resistances in linear motion can be achieved by an increase in the main counterweights, i.e. by an increase in the negative value of the eccentric's static moment over the value which balances the mass inertia resistances in the rotational movement of the main shaft. The distribution of forces acting on the main bearing is presented in Figure 2. It should be emphasised that the resultant force W_i rotates in the opposite direction to that of the crank rotation.

The resistance moments of friction in the main bearing can be determined by the approximate dependency:

$$M_{t_i} = W_i \cdot \mu_i \cdot \frac{d}{2} \qquad i = 1, \ldots, 4 \quad (6)$$

where:

W_i - the rotating resultant force acting on the main bearing which considers the masses in the reciprocating motion and the balancing mass; the resultant force can be described by equation (7), where:

m - part of the mass of the needle-bench (1/4 part of the total mass),

β - the mass balancing coefficient in the reciprocating motion,

μ - the coefficient of friction, and

d - the diameter of the main shaft journal.

Mathematical Model of the System Presented in Figure 1

The mathematical model of the needle bench driving unit is described by the sets of equations describing the action of the asynchronous motor (equations 8-10), the crank-slider system (equations 11-16), the take-up belt wheel (equation 17), and both toothed wheels (equations 18-23). The set of equations (8) which describes the asynchronous motor was accepted in accordance with [11] and formulations described by the Matlab program software. In these equations, $U_{s\alpha}$ and $U_{s\beta}$ are the phase-to phase voltages, L_s, L_w, and L_m the inductivities correspondingly of stator, rotor, and mutual rotor-stator, R_s and R_w the resistivities of stator and rotor, and p - the number of pole pairs; M_{ts} are the constant internal motor resistances, such as for example those resulting from ventilation and friction in the motor bearings, whereas M_0 is the anti-torque at the motor belt wheel formulated by equations (9) and (10), where:

F - the effective belt tension,

S - the belt rigidity coefficient,

D - the belt dumping coefficient,

φ_s - the rotation angle of the motor's rotor,

r_s - the radius of the motor belt wheel,

ψ - the rotation angle of the driven belt wheel, and

r_l - the radius of the driven belt wheel.

The kinematic relations of the crank-slider system are formulated by equations (11-16), where φ_i is the rotation angle of the i-th crank. The dependencies for the take-up belt wheel are described by equation (17), where:

K_l - the coefficient of the transmission shaft's rigidity,

C_l - the coefficient of internal dumping,

ψ_1, ψ_2 - angles of rotation of the belt and toothed wheels, and

I_0 - the belt wheel's mass moment of inertia.

The motion equation of the first toothed wheel of the gear is formulated by the dependency (18), where:

I_k - the mass moment of inertia of the toothed wheel,

K_m - the tooth rigidity,

C_m - the dumping coefficient,

R - the toothed wheel radius,

M_l - the total moment in node A, described by equation (19), where:

I_1 - the mass moment of inertia of the elements fastened in node A_l,

M_{tl} - the moment of friction in the journal bearing,

M_2 - the total moment in node B, described by equation (20), where:

I_2 - the mass moment of inertia of the elements fastened in node B,

M_{t2} - the moment of friction in the journal bearing.

The motion equation of the second toothed wheel of the gear is formulated by the dependency (21), whereas the total moment M_3 in node C is described by equation (22), where:

I_3 - the mass moment of inertia of the elements fastened in node C,

M_{t3} - the moment of friction in the journal bearing,

and the total moment M_4 in node D by equation (23), where:

I_4 - the mass moment of inertia of the elements fastened in node D.

d'Alembert's principle of prepared works, posited individually for each separated crank-slider (eccentric) mechanism, and after taking into account the friction resistances considered as external forces, takes the following form:

$$M_i d\varphi_i + F_{i(t)} dy_i + M_{ti} \cdot d\gamma_i = 0$$

$$i = 1, \ldots, 4 \qquad (24)$$

where:

M_i - the total momentum in the i-th node,

$F_{i(t)}$ - the axial longitudinal force in the i-th node,

$d\varphi_i, dy_i, d\gamma_i$ - the displacements prepared.

After differentiating the formula (24) with respect to φ_i, we obtain the set of relations (25-28).

Results of Numerical Calculation

The mathematical model of the dynamics of the needle-punching machine's driving unit, as formulated by the equations (5-28), has been graphically defined by the Simulink software. A multiple repeated simulation enables the selection of optimal parameters in a real system.

Some coefficients of the mathematical model have been determined during investigation of a simple driving unit. The remaining coefficients, which had been connected with the evolution of the system developed, have been determined from catalogue data, calculated, or based on different measurements.

An example of a simulation analysis of the dynamics of a needle-punching machine's driving unit has been carried out on a real IN2 machine. This machine was developed by and designed under the supervision of the author, and then manufactured by the Befama Machine Manufacturing Enterprise (Bielsko-Bialska Fabryka Maszyn) in co-operation with the Cenaro Research and Development Centre for Textile Machines, Łódź, Poland. The results presented in Figures 3–11 were obtained with the following parameters measured directly from the real object, and selected for computing: r=0.03m, l=0.27m, r_s=0.112m, r_1=0.1575m, I_s=0.167 kgm^2, m=13.665 kg, d=0.085m, d_1=0.048m, β=0.5, R=0.17m, C_m=7×10^3 Ns/m, k_m=8.5×10^8 N/m, λ=0.111, L_s=0.004 H, L_w=0.230 H, L_m=0.226 H, D=200 Ns/m,

$$W_i = \sqrt{\left[m\frac{d^2y_i}{dt^2} - \beta \cdot m \cdot r\left(\frac{d\varphi_i}{dt}\right)^2 \cos\varphi_i\right]^2 + \beta^2 m^2 r^2 \left(\frac{d\varphi_i}{dt}\right)^4 \sin^2\varphi_i} \quad (7)$$

$$\frac{d}{dt}\psi_{w0} = -AL_s R_w \psi_{w0} + AL_m R_w \psi_{\varphi 0} - \omega_s \psi_{w0} \quad (8)$$

$$M_s = S(\varphi_s r_s - \psi_1 r_1) r_s + D\left(\frac{d\varphi_s}{dt} r_s - \frac{d\psi_1}{dt} r_1\right) r_s \quad (9)$$

$$S(\varphi_s r_s - \psi_1 r_1) + D\left(\frac{d\varphi_s}{dt} r_s - \frac{d\psi_1}{dt} r_1\right) = F \quad (10)$$

$$y_i = r\cos\varphi_i + \sqrt{l^2 - (r\sin\varphi_i)^2} \qquad i=1, 2, 3, 4 \quad (11)$$

$$\frac{dy_i}{dt} = \frac{dy_i}{d\varphi_i} \cdot \frac{d\varphi_i}{dt} \qquad i=1, \ldots 4 \quad (12)$$

$$\frac{d^2y_i}{dt^2} = \frac{d}{dt}\left(\frac{dy_i}{d\varphi_i}\frac{d\varphi_i}{dt}\right) = \frac{d^2\varphi_i}{dt^2}\frac{dy_i}{d\varphi_i} + \left(\frac{d\varphi_i}{dt}\right)^2 \frac{d^2y_i}{d\varphi_i^2} \qquad i=1, \ldots 4 \quad (13)$$

$$\frac{dy_i}{d\varphi_i} = -r\sin\varphi_i - \frac{r^2 \sin 2\varphi_i}{2\sqrt{l^2 - (r\sin\varphi_i)^2}} \qquad i=1, \ldots 4 \quad (14)$$

$$\frac{d^2y_i}{d\varphi_i^2} = -r\cos\varphi_i - \frac{r^4\cos^2\varphi_i \sin^2\varphi_i}{\sqrt{(l^2 - r^2\sin^2\varphi_i)^3}} - \frac{r^2\cos^2\varphi_i}{\sqrt{l^2 - r^2\sin^2\varphi_i}} + \frac{r^2\sin^2\varphi_i}{\sqrt{l^2 - (r\sin\varphi_i)^2}} \quad (15)$$

$$\frac{d\gamma_i}{d\tau_i} = \frac{\cos\varphi_i}{\sqrt{1 - \lambda^2\sin^2\varphi}} \quad (16)$$

$$S(\varphi_s r_s - \psi_1 r_1) r_1 + D\left(\frac{d\varphi_s}{dt} r_s - \frac{d\psi_1}{dt} r_1\right) r_1 - k_1(\psi_1 - \psi_2) - C_1\left(\frac{d\psi_1}{dt} - \frac{d\psi_2}{dt}\right) - I_0 \frac{d^2\psi_1}{dt^2} = 0 \quad (17)$$

$$k_1(\psi_1 - \psi_2) + C_1\left(\frac{d\psi_1}{dt} - \frac{d\psi_2}{dt}\right) - I_4 \frac{d^2\psi_2}{dt} - k_2(\psi_2 - \varphi_1) - C_2\left(\frac{d\psi_2}{dt} - \frac{d\varphi_1}{dt}\right) - k_m(R\psi_2 - R\psi_3)R - C_m\left(R\frac{d\psi_2}{dt} - R\frac{d\psi_3}{dt}\right)R = 0 \quad (18)$$

$$M_1 = -I_1\frac{d\varphi_1}{dt^2} - k(\varphi_1 - \varphi_2) - C\left(\frac{d\varphi_1}{dt} - \frac{d\varphi_2}{dt}\right) - k_2(\varphi_1 - \psi_2) - C_2\left(\frac{d\varphi_1}{dt} - \frac{d\psi_1}{dt}\right) - M_{t1} \quad (19)$$

$$M_2 = -I_2\frac{d^2\varphi_2}{dt^2} - k(\varphi_2 - \varphi_1) - C\left(\frac{d\varphi_2}{dt} - \frac{d\varphi_1}{dt}\right) - M_{t2} \quad (20)$$

$$k_m(R\psi_2 - R\psi_3)R + C_m\left(R\frac{d\psi_2}{dt} - R\frac{d\psi_3}{dt}\right)R - I_4\frac{d^2\psi_3}{dt^2} - k_2(\psi_3 - \varphi_3) - C_2\left(\frac{d\psi_3}{dt} - \frac{d\varphi_3}{dt}\right) = 0 \quad (21)$$

$$M_3 = -I_3\frac{d^2\varphi_3}{dt^2} - k_2(\varphi_3 - \psi_3) - C_2\left(\frac{d\varphi_3}{dt} - \frac{d\psi_3}{dt}\right) - k(\varphi_3 - \varphi_4) - C\left(\frac{d\varphi_3}{dt} - \frac{d\varphi_4}{dt}\right) - M_{t3} \quad (22)$$

$$M_4 = -I_4\frac{d^2\varphi_4}{dt^2} - k(\varphi_4 - \varphi_3) - C\left(\frac{d\varphi_4}{dt} - \frac{d\varphi_3}{dt}\right) - M_{t4} \quad (23)$$

Equations 7-23.

S=321,000 N/mrad, I_1=0.4326 kgm^2, I_2=0.4205 kgm^2, I_3=0.4326 kgm^2, I_4=0.4205 kgm^2, μ_1=0.04, μ=0.05, M_{ts}=6.63 Nm, U=380 V, f=24 Hz, A=536.315 H^{-2}, p=1, R_s=0.249 Ω, R_w=0.260 Ω, ω=150.78 s^{-1}, C=8 Nms/rad, k=10.89·10^4 Nm/rad.

The quantitative relations presented were selected while considering these parameters, which are essential for the designer and the exploitation staff.

Conclusions

- The mathematical model of the needle-bench driving unit comprises the dynamics of all the elements applied in modern needle punching machines with crank-slider drives, and is therefore a universal model for this class of needle-punching machines.

$$I_1\frac{d^2\varphi_1}{dt^2} + k(\varphi_1 - \varphi_2) + C\left(\frac{d\varphi_1}{dt} - \frac{d\varphi_2}{dt}\right) + k_2(\varphi_1 - \psi_2) + C_2\left(\frac{d\varphi_1}{dt} - \frac{d\psi_1}{dt}\right) + M_{t1} + \left\{m\left[\frac{d^2\varphi_1}{dt^2}\frac{dy_1}{d\varphi_1} + \left(\frac{d\varphi_1}{dt}\right)^2\frac{d^2y_1}{d\varphi_1^2}\right] + \operatorname{sgn}\left(\frac{dy_1}{dt}\right)T_1 + P_z\right\}\frac{dy_1}{d\varphi_1} + M_{sup}\frac{\cos\varphi_i}{\sqrt{1-\lambda^2\sin^2\varphi}} = 0 \quad (25)$$

$$I_2\frac{d^2\varphi_2}{dt^2} + k(\varphi_2 - \varphi_1) + C\left(\frac{d\varphi_2}{dt} - \frac{d\varphi_1}{dt}\right) + M_{t2} + \left\{m\left[\frac{d^2\varphi_2}{dt^2}\frac{dy_2}{d\varphi_2} + \left(\frac{d\varphi_2}{dt}\right)^2\frac{d^2y_2}{d\varphi_2^2}\right] + \operatorname{sgn}\left(\frac{dy_2}{dt}\right)T_2 + P_z\right\}\frac{dy_2}{d\varphi_2} + M_{sup}\frac{\cos\varphi_i}{\sqrt{1-\lambda^2\sin^2\varphi}} = 0 \quad (26)$$

$$I_3\frac{d^2\varphi_3}{dt^2} + k_2(\varphi_3 - \psi_3) + C_2\left(\frac{d\varphi_3}{dt} - \frac{d\psi_3}{dt}\right) + k(\varphi_3 - \varphi_4) + C\left(\frac{d\varphi_3}{dt} - \frac{d\varphi_4}{dt}\right) + M_{t3} + \left\{m\left[\frac{d^2\varphi_3}{dt^2}\frac{dy_3}{d\varphi_3} + \left(\frac{d\varphi_3}{dt}\right)^2\frac{d^2y_3}{d\varphi_3^2}\right] + \operatorname{sgn}\left(\frac{dy_3}{dt}\right)T_3 + P_z\right\}\frac{dy_3}{d\varphi_3} + M_{sup}\frac{\cos\varphi_i}{\sqrt{1-\lambda^2\sin^2\varphi}} = 0 \quad (27)$$

$$I_4\frac{d^2\varphi_4}{dt^2} + k(\varphi_4 - \varphi_3) + C\left(\frac{d\varphi_4}{dt} - \frac{d\varphi_3}{dt}\right) + M_{t4} + \left\{m\left[\frac{d^2\varphi_4}{dt^2}\frac{dy_4}{d\varphi_4} + \left(\frac{d\varphi_4}{dt}\right)^2\frac{d^2y_4}{d\varphi_4^2}\right] + \operatorname{sgn}\left(\frac{dy_4}{dt}\right)T_4 + P_z\right\}\frac{dy_4}{d\varphi_4} + M_{sup}\frac{\cos\varphi_i}{\sqrt{1-\lambda^2\sin^2\varphi}} = 0 \quad (28)$$

Equations 25-28.

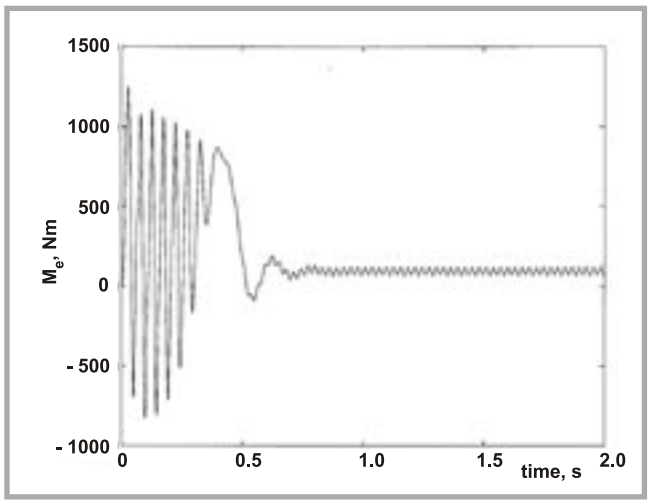

Figure 3. *Electromagnetic momentum of the motor, start-up run.*

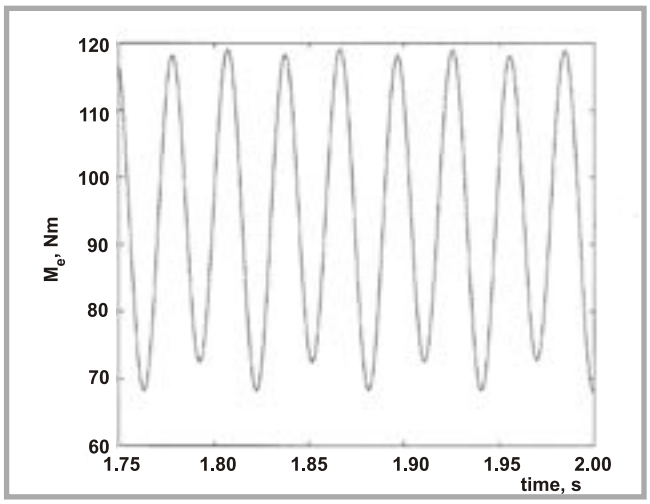

Figure 4. *Electromagnetic momentum of the motor, stationary state.*

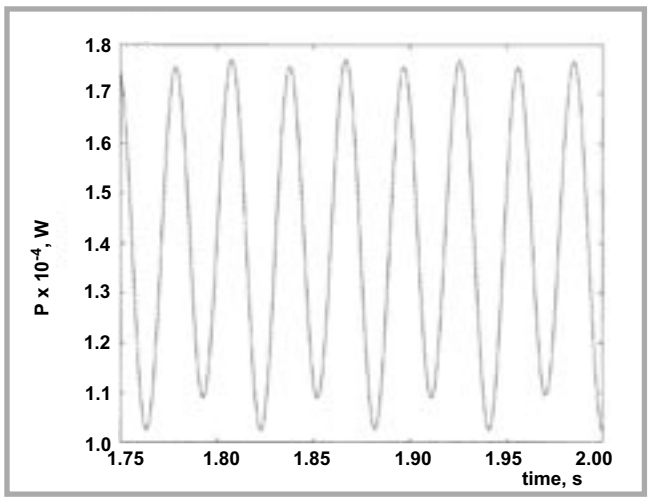

Figure 5. *Mechanical power of the motor, stationary state.*

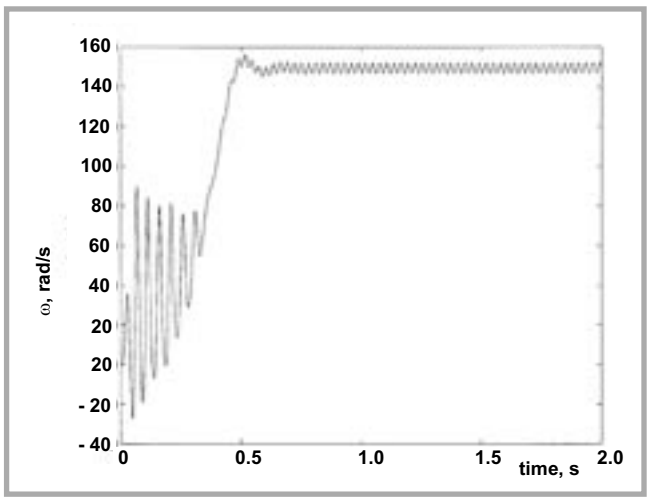

Figure 6. *Rotational velocity of the motor, start-up run.*

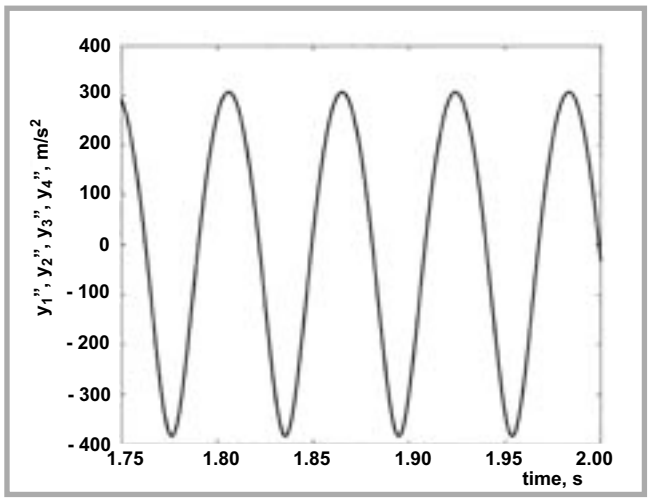

Figure 7. *Linear acceleration, stationary state.*

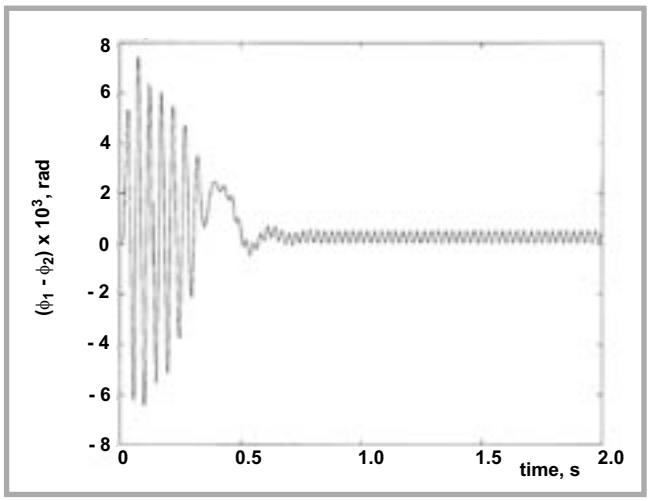

Figure 8. *Shift twist angle I, start-up run*

- The mathematical model can be developed by the addition of successive needling modules, and in this way a model of a machine with optional width can be formed.
- The simulation model allows us to investigate a broad range of the model's parameter changes.

References

1. *Kapusta H., Dynamics of needling and of the mechanisms of a needling punching machine (in Polish), Scientific Letters of*

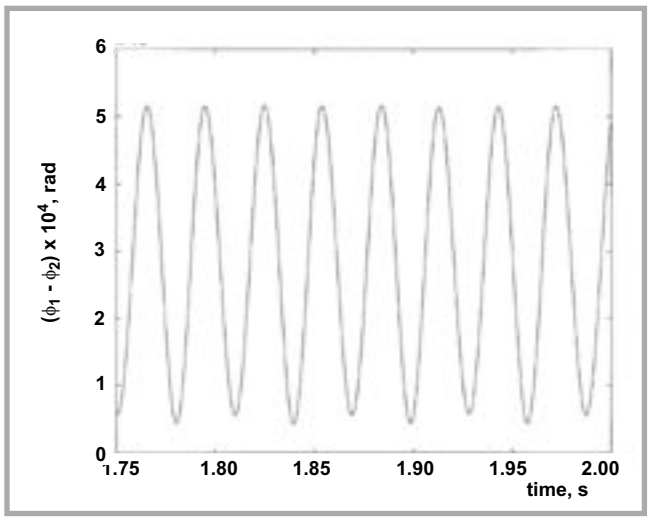

Figure 9. *Shift twist angle I, stationary state.*

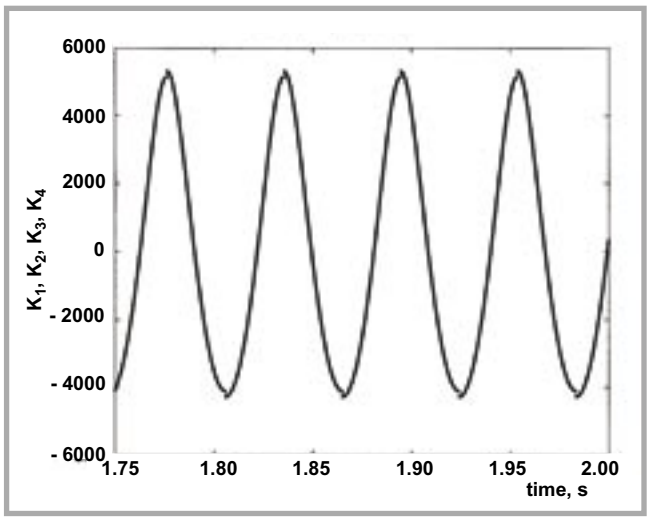

Figure 10. *Curve of the forces K_i (K_1, ..., K_4) in the connector rod.*

the Technical University of Łódź, No. 917, Scientific Dissertations, L. 318, 2002.

2. *Zajączkowski J., Torsion Vibrations of Shafts in a Sewing Machine, Fibres & Textiles in Eastern Europe, Vol. 4, No 3-4/1996, pp. 49-50.*
3. *Zajączkowski J., Dynamics of Mechanisms Driving a Needle and a Hook in a Sewing Machine, Scientific Letters of the Technical University of Łódź, L. 54, No. 760, pp. 5-12, 1996.*
4. *Golebiewski E.P., Sadler I.P., Analytical and experimental investigation of elastic slider-crank mechanisms, Journal of Engineering for Industry, pp. 1266-1271, 1976.*
5. *Zajączkowski J., Torsion Vibrations of a Hook Shaft in a Sewing Machine, Fibres & Textiles in Eastern Europe, vol. 7, No 1/1999, pp. 51-53.*
6. *Kapusta H., Analysis of Kinetic Phenomena during the needling process of textile fleece (in Polish), Proceedings of the 2nd Scientific Conference of the Textile Faculty, Technical University of Łódź, 1998, pp.25-26.*
7. *Kapusta H., Dynamics analysis of the operation of a needle punching machine (in Polish), research report, Technical University of Łódź.*
8. *Kapusta H., Mathematical model of the needle punching machine (in Polish), Proceedings of the 3rd Scientific Conference of the Textile Faculty, Technical University of Łódź, 2000, pp. 1-4.*
9. *Kapusta H., Mathematical model of the needle punching machine as the basis for a simulation diagnostic (in Polish), Proceedings of the 27th All-Polish Symposium for Machine Diagnostic, Węgierska Górka, in Scientific Letters of the Silesian Technical University, No. 2, pp.135 138, 2000.*
10. *Kapusta H., Strzelecki S., Numerical Analysis of Needle Punching Machine Journal Bearings Operation, Proceedings of the International Textile Conference IMTEX'2000, and Scientific Letters of the Technical University of Łódź, No. 58, pp. 341-347, 2000.*
11. *Bielawski S., Teoria napędu elektrycznego, WNT, Warsaw, 1978.*

Received 16.04.2004 Reviewed 12.05.2004